A Method to Increase the Field of View of an Imaging Optical System

Lin Sun, Qingfeng Cui, Zhen Zong, Mingxu Piao, and Bo Zhang

***Abstract*—The Y field of view of an off-axis optical system is generally less than 1°. Scholars usually use a freeform surface to achieve a rectangular field of view imaging. However, it adds to the difficulty of processing, testing, assembling, and adjusting, and at the same time has the drawbacks of high manufacturing costs and long processing cycles. In view of the above problems, this paper presents a computational imaging design method for expanding the Y field of view of an off-axis optical system. This method analyzes the aberration characteristics of the optical system, creates a point spread function model based on the wavefront aberration theory and Zernike polynomials, and processes images using a spatial variation deconvolution algorithm. In this paper, we used this method to simulate an off-axis three-mirror optical system with a focal length of 260 mm, the f-number of 2.5, and a field of view of 8° × 1° and compare the images before and after processing. The results show that the processed images have a clear outline, the overall image quality is improved, the field of view is improved to 8° × 6°, and the modulation transfer function of the entire field of view is above 0.4. The off-axis optical system rectangular field of view imaging is realized without using a freeform surface.**

***Index Terms*—Optical design, off-axis optical system, computational imaging, Point Spread Function (PSF).**

I. Introduction

THE off-axis optical system has many advantages, such as no chromatic aberration, large aperture, no central obscuration, foldable optical system, easy lightweight, and low sensitivity to temperature and air pressure [1]–[4]. Since the 1990s, off-axis three-mirror optical systems have been developed and improved rapidly [5], [6]. Such systems have been used in aviation and space observation systems in many countries, especially in new generation space optical remote sensing [7], [8]. The demand for optical system resolution has increased, and it is difficult to solve the problem. Therefore, it is necessary to study the off-axis three-mirror optical systems.

The traditional off-axis three-mirror optical systems make the elements eccentric and off-axis processing to achieve no central obstruction. Generally, the off-axis three mirror optical system consists of three mirrors. The surface of the primary mirror is usually hyperboloid, the secondary mirror is standard conic surface, and the tertiary mirror is even aspheric surface. The optical system is symmetric in the X field of view and asymmetric in the Y field of view. The field of view of the optical system can be more than 10° in the X-direction. However, because of the off-axis aberration in the Y-direction, it is difficult to make the field of view very large, generally less than 1° [5]–[10]. This requires a linear array detector to receive the image and obtain the rectangular field of view by scanning and swinging [10]. In order to realize the imaging of an off-axis three-mirror optical system with a rectangular field of view (expanding the field of view in the Y-direction), scientists use free-form surface optical elements in the system to correct off-axis aberrations and increase the field of view [11]–[18]. Optical free-form surface is a non-rotational symmetric surface, which is different from the traditional surface types such as spherical surface, quadric surface and even aspheric surface. However, the use of free-form mirrors in optical systems also introduces new problems. The difficulty of processing, inspection, assembly, and adjustment is significantly increased, the manufacturing cost is expensive, the production cycle is long, the difficulty of optical design is high, and errors are difficult to control [19].

Therefore, a new method is needed to enlarge the Y field of view of the off-axis optical systems. In recent years, computational imaging technology has developed rapidly [20]–[23]. It redefines the imaging method, which can improve the problems in traditional optical systems, such as realizing the complete focus imaging of conventional cameras, improving the imaging quality of simple optical systems, and solving the problem of diffraction efficiency degradation of diffractive elements [24]–[26]. In this paper, a method is proposed based on computational imaging to enlarge the Y field of view of the off-axis three-mirror optical systems. First, we analyzed the aberration characteristics of an off-axis three-mirror optical system. Based on the wavefront aberration theory and Zernike polynomials, we propose a wavefront aberration construction method for asymmetric optical systems, establish a wavefront aberration model, and construct a generalized pupil function. Next, a Fourier transform is performed on the generalized pupil function, the PSF (Point Spread Function) is obtained by taking the square of the transformation result modulus, and the PSF model is established. A spatial variation deconvolution algorithm and the PSF model are used to process the image. Finally, the blur caused by a large field of view aberration is eliminated, and the rectangular field of view imaging is realized. We simulated a typical off-axis three-mirror optical system and used this method

Manuscript received September 16, 2021; revised November 23, 2021; accepted November 30, 2021. Date of publication December 3, 2021; date of current version December 17, 2021. This work was supported by the National Science and Technology Major under Project 51-H34D01-8358-13/16 *(Corresponding author: Qingfeng Cui.)*

The authors are with the School of Opto-Electronic Engineering, Changchun University of Science and Technology, Changchun 130022, China (e-mail: aa4661583@163.com; qfcui163@163.com; zongzhen163@126.com; piaomingxu163@163.com; zhangbo1632021@163.com).

Digital Object Identifier 10.1109/JPHOT.2021.3132344

to process images. According to the results, the contour of the processed image is clear, and the Y field of view of the off-axis three-mirror optical system can be expanded without using a freeform surface. This study provides a new idea for the design of an off-axis optical system.

II. Basic Principles

The imaging of an optical system can be understood as the process of convolution between the object and the PSF of the system, which can be expressed as follows [27]:

$$g(x,y) = h(x,y) \otimes f(x,y) + \eta(x,y) \tag{1}$$

where f (x, y) is the object, h (x, y) is the PSF of the optical system, η (x, y) is the noise, g (x, y) is the image, and $\otimes$ is the convolution operation. In the case of little noise, if the object and the optical system remain unchanged, the image will not change. This means that there is a one-to-one correspondence between objects and images in the same optical system. Therefore, if the image and the PSF are known, and the noise is suppressed, the object can be obtained.

A. Aberration Analysis of Off-Axis Three-Mirror Optical System

In the off-axis reflection optical system, since there is no lens, the main aberrations are monochromatic aberrations, which need to be especially considered for correction. Compared to axisymmetric systems, because of the inclination and eccentricity of the mirror, the aberrations produced by the off-axis reflection system in each plane have spatial and directional characteristics [28].

Since the off-axis reflective optical system does not produce chromatic aberrations, the main aberrations corrected by the optical system are the spherical aberration, coma, astigmatism, field curvature, and distortion. The tilt and eccentricity of the element do not affect spherical aberrations. High-power aberrations affect all low-power aberrations [41]. For example, eccentric spherical aberration affects eccentric coma, astigmatism, field curvature, and distortion. Similarly, eccentric astigmatism affects field curvature and distortion [29].

The number of surfaces that a reflective optical system can effectively use is limited, so the aspheric surface is often used for aberration corrections. The aberration correction of reflective optical systems mostly uses quadric surface, aspheric surface, and special free-form surface for aberration correction. At present, the most widely used method is to use the special properties of Zernike free-form surface polynomials to correct the large field of view off-axis aberrations.

B. Principles of Establishing PSF Model

The purpose of building a PSF model is to obtain the speckle with energy intensity information. The ray-tracing method (Ray-tracing is a "general technology from geometric optics. It obtains the path model of light by tracing the light interacting with the optical surface".) can be used to obtain the dispersed spots, but the effect of aperture diffraction cannot be considered in ray-tracing. In the actual imaging process, the effect of diffraction on imaging is significant and cannot be ignored. In order to be more consistent with the actual imaging process, this paper uses Zernike polynomials, wavefront aberration, and generalized pupil function to build the PSF model. Compared to ray tracing, this method considers the effect of diffraction on speckle and improves the construction speed of the model.

TABLE I
First Nine Terms of Fringe Zernike Polynomial Expansion

Term	Zernike polynomial	Name
Z_1	1	Piston
Z_2	$R\cos\theta$	*X*-tilt
Z_3	$R\sin\theta$	*Y*-tilt
Z_4	$2R^2$-1	Defocus
Z_5	$R^2\cos 2\theta$	X-astigmatism
Z_6	$R^2\sin 2\theta$	Y-astigmatism
Z_7	$(3R^3\text{-}2R)\cos\theta$	*X*-coma
Z_8	$(3R^3\text{-}2R)\sin\theta$	*Y*-coma
Z_9	$6R^4\text{-}6R^2\text{+}1$	Spherical aberration

R and θ in Table I represent polar radius and polar angle in polar coordinates, respectively.

The pupil function p (x, y) of the off-axis three-mirror optical system is expressed as:

$$p(x,y) = \begin{cases} 1, & x^2 + y^2 \le \rho^2 \\ 0, & \text{otherwise} \end{cases} \tag{2}$$

where (x, y) is the pupil coordinate, and ρ is the pupil radius.

The pupil function can only represent the shape of the incident beam and does not include the optical system aberration. In order to characterize the aberration of an optical system, the generalized pupil function P (x, y) is introduced:

$$P(x,y) = p(x,y)\exp[ikW(x,y)] \tag{3}$$

where the wavenumber $k = \frac{2\pi}{\lambda}$, λ (nm) is wavelength, W (x, y) represents the optical path difference of the actual wave surface from the ideal spherical surface, which is called wavefront aberration. The wavefront aberration of an optical system can be expressed by the linear combination of Zernike polynomial Z_i [30]:

$$W(x,y) = \sum_{i=1}^{\infty} a_i Z_i \tag{4}$$

where a_i is the coefficient of Zernike term and i is polynomial order. The Zernike polynomials have a corresponding relationship with the Seidel aberrations. The corresponding aberrations of the first nine Zernike polynomials are shown in Table I. Fig. 1 shows the wavefront error distribution with different Zernike coefficients. For example, if there is defocus in the system, we can express this defocus amount with Z4 [32], [33].

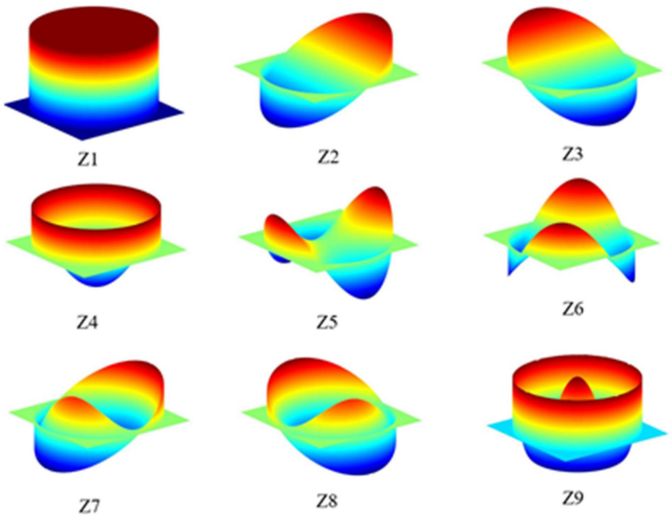

Fig. 1. Wavefront error distribution with different Zernike coefficients.

The Zernike polynomials can be used to express wavefront aberrations of optical systems, as shown in (5):

$$W(x,y) = \sum_{i=1}^{9} a_i Z_i + \sum_{j=10}^{\infty} a_j Z_j \tag{5}$$

where $\sum_{j=10}^{\infty} a_j Z_j$ is the wavefront aberration compensation term. When the optical system focal length is small, this term represents the wavefront aberration of advanced aberrations. In order to get the wavefront aberration expression W (x, y) of the optical system, we need to analyze various aberrations of the optical system according to the corresponding relationship between the Zernike polynomials and Seidel aberrations (as shown in Table I) and obtain the coefficients of Zernike terms to get the wavefront aberration expression.

For the off-axis reflective optical system, the optical system is asymmetric. Hence, it is difficult to construct the wavefront aberration in a single direction as the coaxial optical system and obtain As a result, we need to construct directly in the whole field of view, and the construction method is shown in (6) at the bottom of this page, where *xx* and *yy* are the coordinates of the normalized field of view of the systems X and Y, respectively. m and n are the sampling steps of the normalized field of view of the systems X and Y, respectively. Then the Zernike coefficient matrix is brought into (7), and the wavefront aberration of the optical system can be obtained as follows:

$$W(x,y) = [A_1(xx,yy), A_2(xx,yy), A_3(xx,yy), \cdots A_i(xx,yy)] \times Z_i \tag{7}$$

where $Z_i = [Z_1, Z_2, Z_3, \ldots Z_i]^T$.

Fig. 2 provides a better understanding of the wavefront aberration calculation process. As shown in Fig. 2, given that the detector resolution is 4×4 (practically, it is calculated according to the actual detector resolution), we can calculate the wavefront aberration pixel by pixel. Finally, we can get the wavefront aberration by superposition.

Since the coefficients of the Zernike terms obtained in (6) are originally matrices, the wavefront aberrations of each field of view can be introduced directly into (7) without rotation. This method is slow to obtain the wavefront aberration of an optical system. Therefore, we can consider the Zernike coefficients corresponding to the special field of view point and fit it with polynomial to get the function relation about the Zernike coefficients F (a, x, y), which can significantly reduce the speed of model construction and improve efficiency.

The generalized pupil function of the system can be obtained by introducing the obtained W (x, y) into (3). The generalized pupil function is transformed by the Fourier transform, and the square of the transformation result is PSF, which can be expressed as follows:

$$f_{PSF}(x,y) = |\mathcal{F}\{P(x,y)\}|^2 \tag{8}$$

where $\mathcal{F}$ is the Fourier transform. The PSF model of the optical system can be constructed by introducing the generalized pupil function of each field of view into (8).

C. Spatial Variation Deconvolution Algorithm

The deconvolution algorithm ignores the characteristics of fuzzy kernel changing with space and uses the same fuzzy kernel to deconvolute the whole image. Fuzzy kernel is a parameter that causes image blur. In optical system, fuzzy kernel is PSF. It has a certain accuracy when the fuzzy kernel slightly changes. This method is called the space invariant deconvolution algorithm. The spatial variation deconvolution algorithm must be used for the system whose blur kernel changes significantly with space. Because of off-axis aberration in the off-axis three-mirror optical system and the limited degree of freedom of the system, it is impossible to correct all aberrations. Therefore, the spatial variation deconvolution theory proposed by Filip Sroubek is adopted in this paper [30]. This method can process images affected by all aberrations. The traditional spatial invariant deconvolution algorithm can only deal with images affected by only one aberration.

$$A_i(xx,yy) = \begin{bmatrix} a_i(-1,-1) & a_i(-1+m,-1) & \cdots a_i(0,-1) & \cdots a_i(1,-1) \\ a_i(-1,-1+n) & a_i(-1+m,-1+n) & \cdots a_i(0,-1+n) & \cdots a_i(1,-1+n) \\ \vdots & \vdots & \vdots & \vdots \\ a_i(-1,0) & a_i(-1+m,0) & \cdots a_i(0,0) & \cdots a_i(1,0) \\ a_i(-1,0+n) & a_i(-1+m,0+n) & \cdots a_i(0,0+n) & \cdots a_i(1,0+n) \\ \vdots & \vdots & \vdots & \vdots \\ a_i(-1,1) & a_i(-1+m,1) & \cdots a_i(0,1) & \cdots a_i(1,1) \end{bmatrix} \tag{6}$$

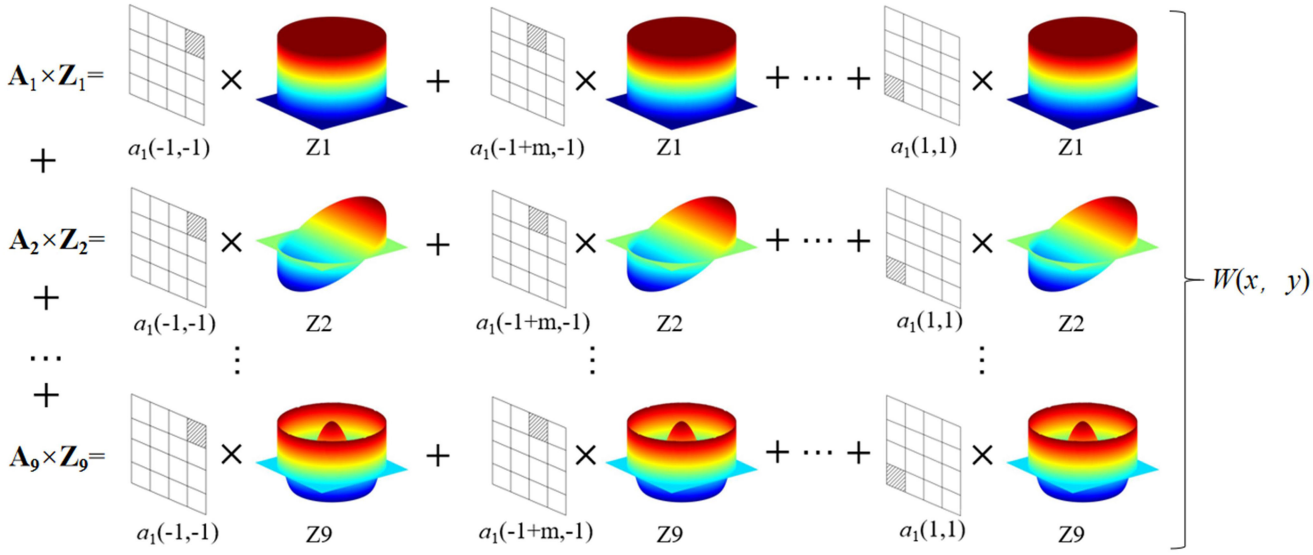

Fig. 2. Schematic diagram of wavefront aberration calculation.

In this theory, the fuzzy kernel is singularly decomposed into the base filter matrix $\boldsymbol{B} = [\boldsymbol{B}_1, \boldsymbol{B}_2, \ldots, \boldsymbol{B}_k]$ and the coefficient matrix $\boldsymbol{M} = [\boldsymbol{M}_1, \boldsymbol{M}_2, \ldots, \boldsymbol{M}_k]$, as shown in (9):

$$\boldsymbol{PSF} = [\boldsymbol{B}_1, \boldsymbol{B}_2, \ldots, \boldsymbol{B}_k] \begin{bmatrix} \boldsymbol{M}_1 \\ \boldsymbol{M}_2 \\ \vdots \\ \boldsymbol{M}_k \end{bmatrix} \tag{9}$$

k means to arrange the singular values from large to small and take the first k singular values. The larger the k value, the better the restoration effect and the slower the restoration speed. By substituting (9) into (1), we can obtain:

$$\boldsymbol{g} = [\boldsymbol{B}_1, \boldsymbol{B}_2, \ldots, \boldsymbol{B}_k] \begin{bmatrix} \boldsymbol{M}_1 \\ \boldsymbol{M}_2 \\ \vdots \\ \boldsymbol{M}_k \end{bmatrix} * \boldsymbol{f} + \boldsymbol{\eta} \tag{10}$$

In order to solve (10), we use the idea of normalization to find the optimal solution. The optimal evaluation criteria can be expressed as follows:

$$\arg\min \left\{ \left\| f_{PSF} * \hat{\boldsymbol{f}} - \boldsymbol{g} \right\|_2^2 + \gamma \left\| \nabla^2 \hat{\boldsymbol{f}} \right\|_p \right\} \tag{11}$$

where $\| f_{PSF} * \hat{\boldsymbol{f}} - \boldsymbol{g} \|_2^2$ is the fidelity term, $\| \nabla^2 \hat{\boldsymbol{f}} \|_p$ is a smooth constraint term used to suppress noise and ringing effect, $\hat{\boldsymbol{f}}$ is the approximate solution of the object, $\boldsymbol{g}$ is the image received by the detector, γ is the weights of smooth constraints, $\boldsymbol{C}$ is the Laplacian Operator, and p corresponds to different norm types. Finally, we use the ADMM (alternating direction method of multipliers) method to obtain the optimal solution $\hat{\boldsymbol{f}}$ of (11) and complete the image restoration.

To sum up, the process of this method is as follows. First, the off-axis three-mirror optical system is taken into account as the initial structure, and the system is preliminarily optimized without using a free-form surface. Next, the optical system is sampled, the point diffusion function model at each sampling point is approximated by the Zernike polynomial, and the fitting coefficients are obtained. (3) and (4) are combined to calculate the wavefront aberration and construct the generalized pupil function, and the Fourier transform is used to obtain the PSF model. Finally, the theory proposed by Filip Sroubek [30] and others is used to decompose the PSF model established in the previous step by a singular value to obtain the base filter matrix **B** and the coefficient matrix **M.** Combined with the blurred image g received by the detector, it is possible to establish (11). The flow chart of the method is shown in Fig. 3.

TABLE II
DESIGN SPECIFICATIONS OF THE SYSTEM

Parameters	Content
Focal length/mm	260
F-number	2.5
Wavelength/nm	400–700
Field of view/ (°)	8°×1°
Expected field of view/ (°)	8°×6°

III. DESIGN EXAMPLES

A. Optical System Design

In a traditional off-axis three-mirror optical system, the field of view in Y-direction is generally less than 1° without using a free-form surface. An off-axis three-mirror optical system in the 8° × 1° field of view is selected for the analysis. After optimization, the technical indexes of the designed optical system are shown in Table II, and the optical system is shown in Fig. 4(a).

In the NSC0806 visible light detector with a resolution of 768 × 576 and the pixel size of 10 μm, the optical system was optimized, and the field of view was increased to 6° to match the

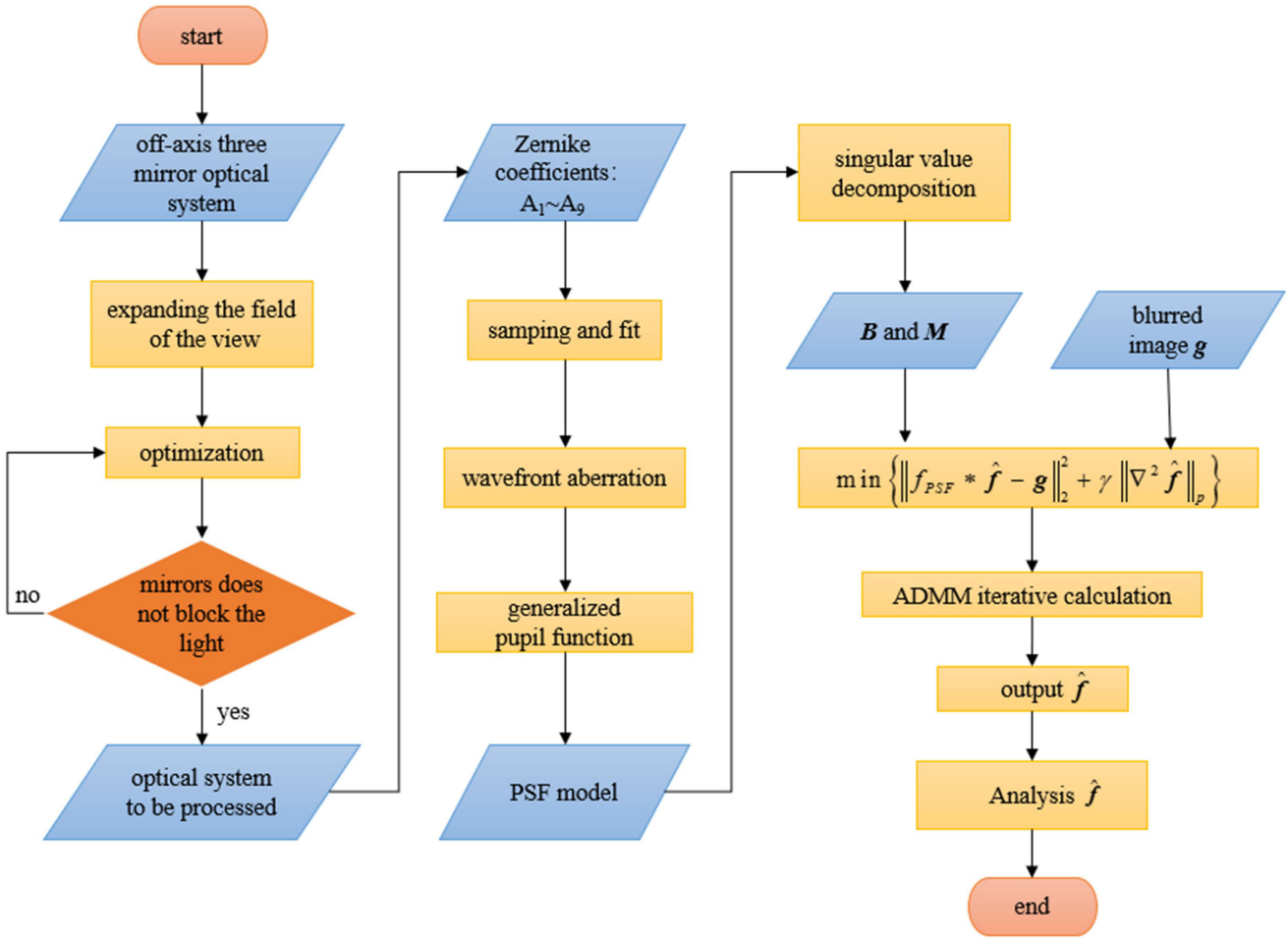

Fig. 3. The flow chart of the method used in this study.

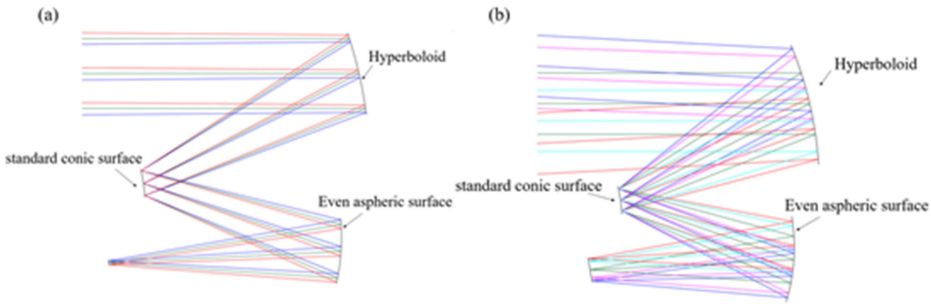

Fig. 4. Optical system diagram (a) Y field of view is 1° and (b) Y field of view is 6°.

length-width ratio of the detector. In the optimization process, it is necessary to increase the distance (Y-direction) between the upper edge of the secondary mirror and the lower edge of the main mirror while expanding the field of view to ensure that the secondary mirror does not block the incident light, as shown in Fig. 4(b).

After optimization, the primary mirror is hyperboloid, the secondary mirror is quadric, and the third mirror is even aspheric. Since the optical system is symmetrical in the plane YOZ, the positive X-direction field of view needs to be analyzed. The spot diagram of the system is shown in Fig. 5.

B. Establishing PSF Model

According to the method mentioned in Section II-B, the X normalized field of view is taken as (0, 0.7, 1), and the Y normalized field of view is taken as (−1, −0.7, 0, 0.7, 1), with 15 field points for simulation analysis. The Zernike coefficients corresponding to 15 fields of viewpoints are fitted according to Cubic Griddata fitting method polynomials, and the fitting error SSE (sum-squared error, The closer SSE is to 0, the better the model selection and fitting, and the more successful the data prediction is.) is less than 0.00002. Fig. 6 shows the surface fitting results of the Zernike coefficients A_1~A_9.

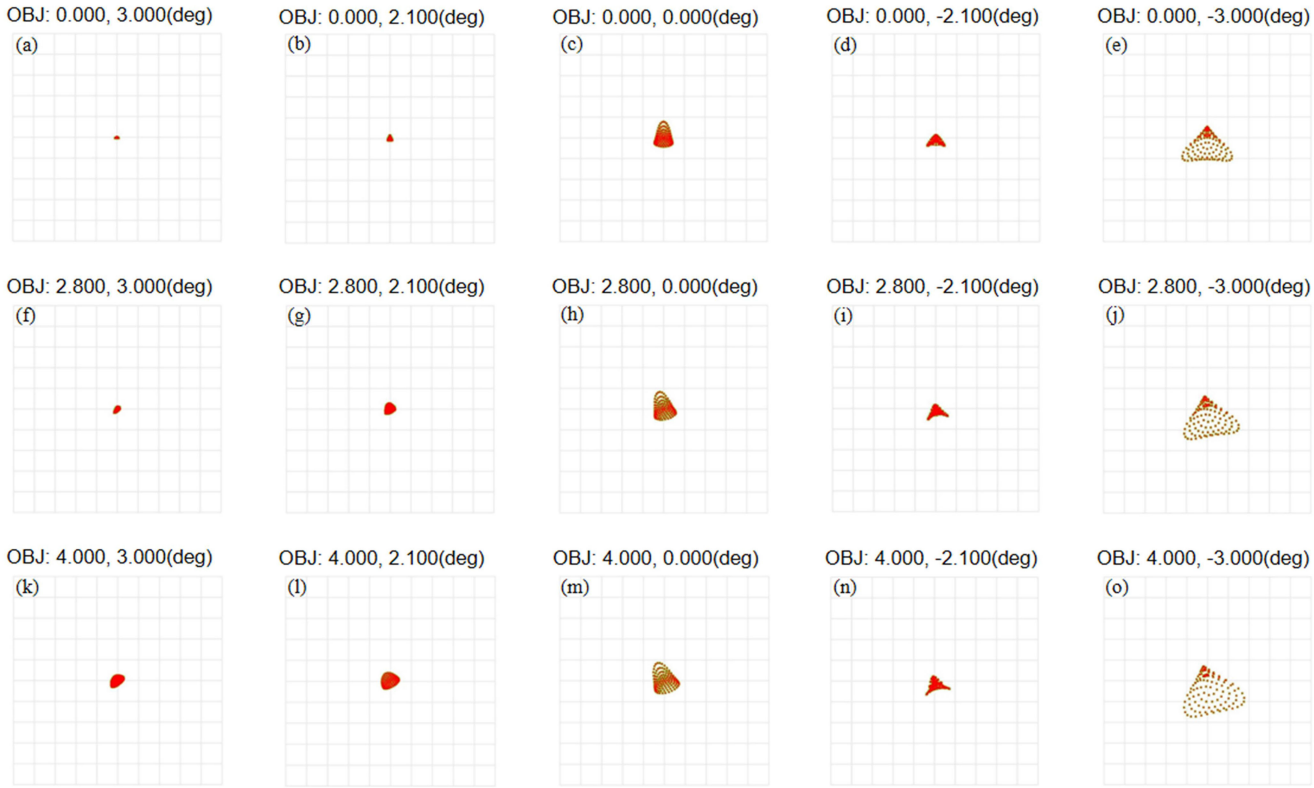

Fig. 5. The spot diagrams of each field of view of the optical system: (a)–(e) are the spot diagrams corresponding to different Y fields of view when X field of view is 0°; (f)–(j) are the spot diagrams corresponding to different Y fields of view when X field of view is 2.8°; (k)–(o) are the spot diagrams corresponding to different Y fields of view when X field of view is 4°.

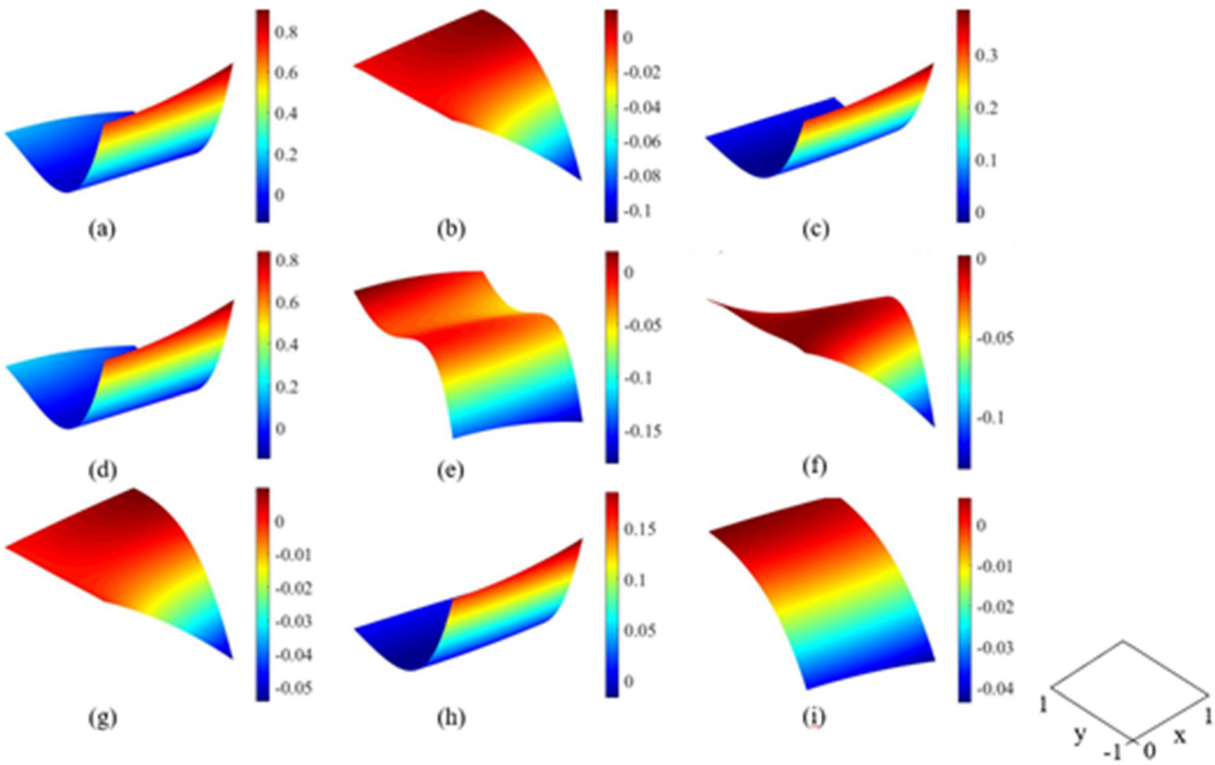

Fig. 6. Zernike polynomial coefficients: (a)–(i) correspond to coefficients a1–a9 respectively, X and Y are the normalized field of view of the optical system, $X \in [01]$, $Y \in [-11]$.

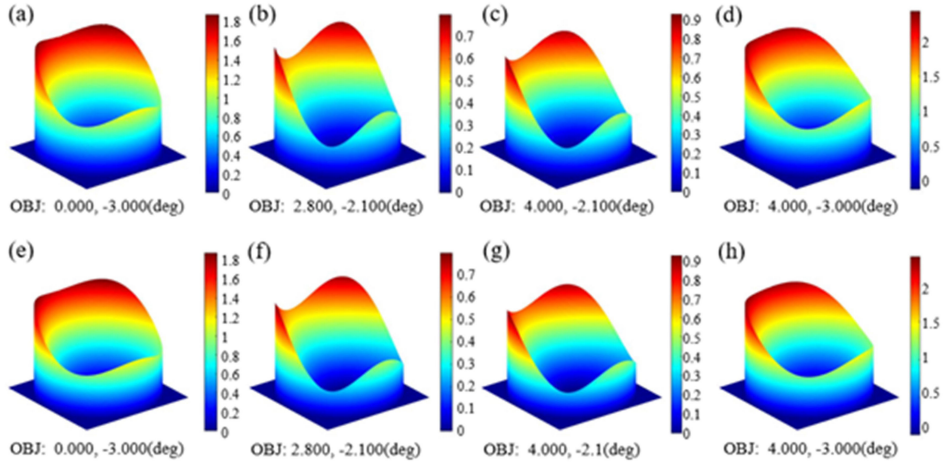

Fig. 7. Wavefront comparison of off-axis three-mirror optical systems. The wavefront figure calculated by ZEMAX: (a) (0°, −3°), (b) (2.8°, −2.1°), (c) (4°, −2.1°), (d) (4°, −3°); the wavefront figure calculated by the model: (e) (0°, −3°), (f) (2.8°, −2.1°), (g) (4°, −2.1°), (h) (4°, −3°).

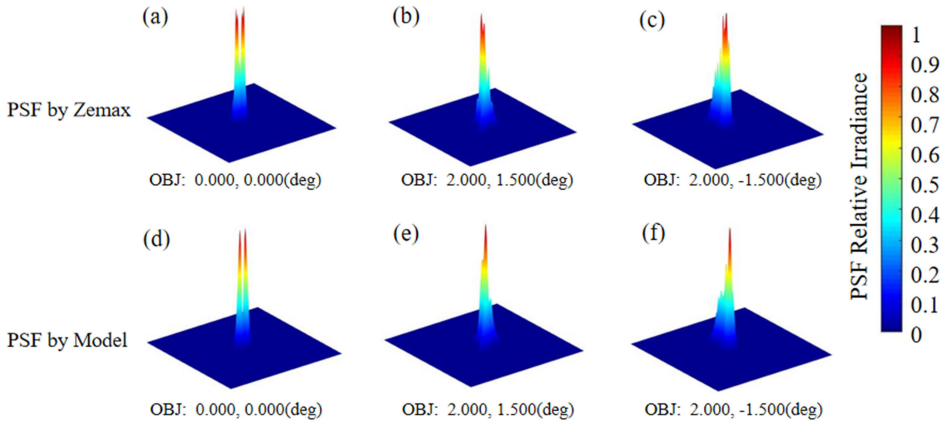

Fig. 8. PSF comparison of off-axis three-mirror optical system. The PSF calculated by ZEMAX: (a) (0°, −2.1°), (b) (2.8°, −2.1°), (c) (4°, −2.1°); the PSF calculated by the model: (d) (0°, −2.1°), (e) (2.8°, −2.1°), (f) (4°, −2.1°).

In order to obtain the continuous wavefront aberration model, the fitting surface Equation in Fig. 6 is introduced into (7) to establish the wavefront aberration model. According to Fig. 5, the imaging quality gradually decreases when the Y field of view decreases from 3° to −3°. Therefore, we focus on the case when the Y field of view is less than zero. As shown in Fig. 7, we extracted four field points (0, −3) (2.8, −2.1) (4, −2.1) and (4, −3) and compared the wavefront aberrations calculated by ZEMAX with those of the constructed model.

Fig. 7(a)–(d) are the wavefront diagrams calculated by ZEMAX software, and Fig. 7(e)–(h) are the wavefront diagrams calculated by the established model. The difference between them is relatively small, so the models constructed are accurate.

By substituting the wavefront aberration model into (3), the generalized pupil function of the optical system is obtained. Then, by substituting the generalized pupil function into (8), the PSF model is finally obtained. As shown in Figs. 8 and 9, six fields of viewpoints (0, −2.1) (2.8, −2.1) (4, −2.1) (0, −3) (2.8, −3) (4, −3) were extracted, and the PSF calculated by ZEMAX was compared with the PSF calculated by the model.

Fig. 8(a)–(c) show the PSF calculated by ZEMAX and the PSF calculated by the model (Fig. 8(d)–(f)) for different X fields of view at y −2.1°. Fig. 9(a)–(c) show the PSF calculated by ZEMAX and the PSF (Fig. 9(d)–(f)) calculated by the model for different X fields of view at Y −3°. A slight deviation can be found between the PSF calculated by ZEMAX and the PSF calculated by the model. The reason for this phenomenon is the influence of high-order Zernike coefficients. In this model, the high-order Zernike coefficients (above the 9th term) slightly affect the imaging quality and are ignored to improve the operation efficiency.

IV. Results and Analysis

The PSF model calculated in Section III-B was used to process the blurred images received by the detector using the spatial variation deconvolution algorithm described in Section II-C. Because the optical system works in the visible band, it needs to be processed in different channels. Since the algorithm is used to calculate the value of the image, the color image is composed of a three-numerical RGB matrix. Hence, the image is decomposed into RGB three channels, respectively, to build the PSF model, process the RGB three-channel graphics synthesis, and finally obtain the processed color graphics. To evaluate the quality of the

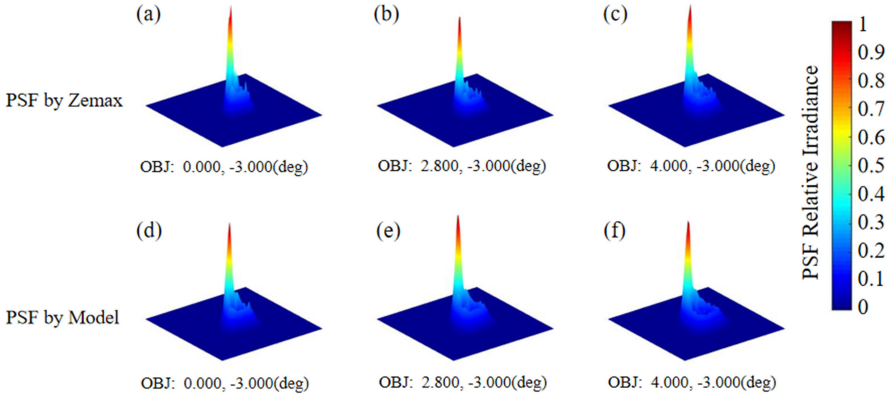

Fig. 9. PSF comparison of off-axis three-mirror optical system. The PSF calculated by ZEMAX: (a) (0°, −3°), (b) (2.8°, −3°), (c) (4°, −3°); the PSF calculated by the model: (d) (0°, −3°), (e) (2.8°, −3°), (f) (4°, −3°).

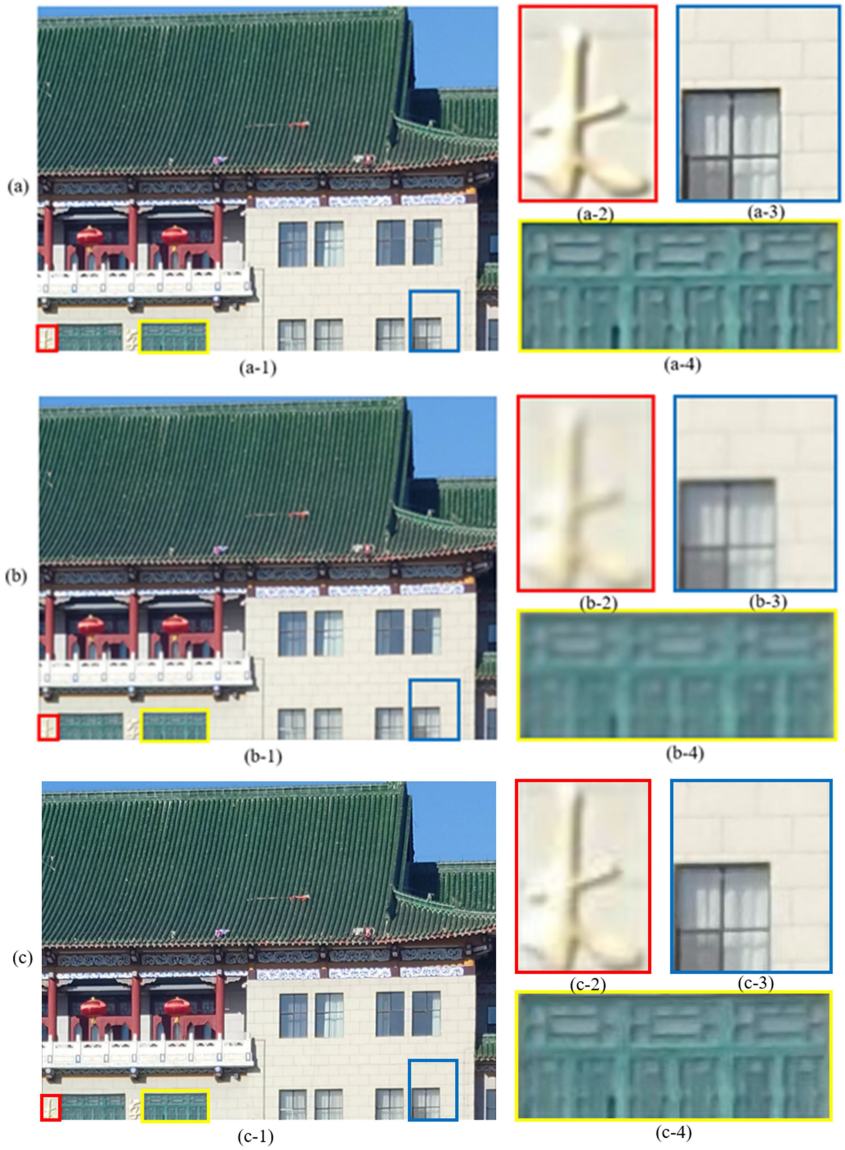

Fig. 10. Comparison before and after restoration. (a) original image, (a-1) is the original image captured, (a-2), (a-3), and (a-4) are the local enlarged images of (a-1); (b) imaging simulation image, (b-1) is the imaging simulation image of (a-1) through the optical system, (b-2), (b-3), and (b-4) are the local enlarged images of (b-1); (c) restoration image, (c-1) is the image restored according to the constructed model, (c-2), (c-3), and (c-4) are the partial enlargement of (c-1).

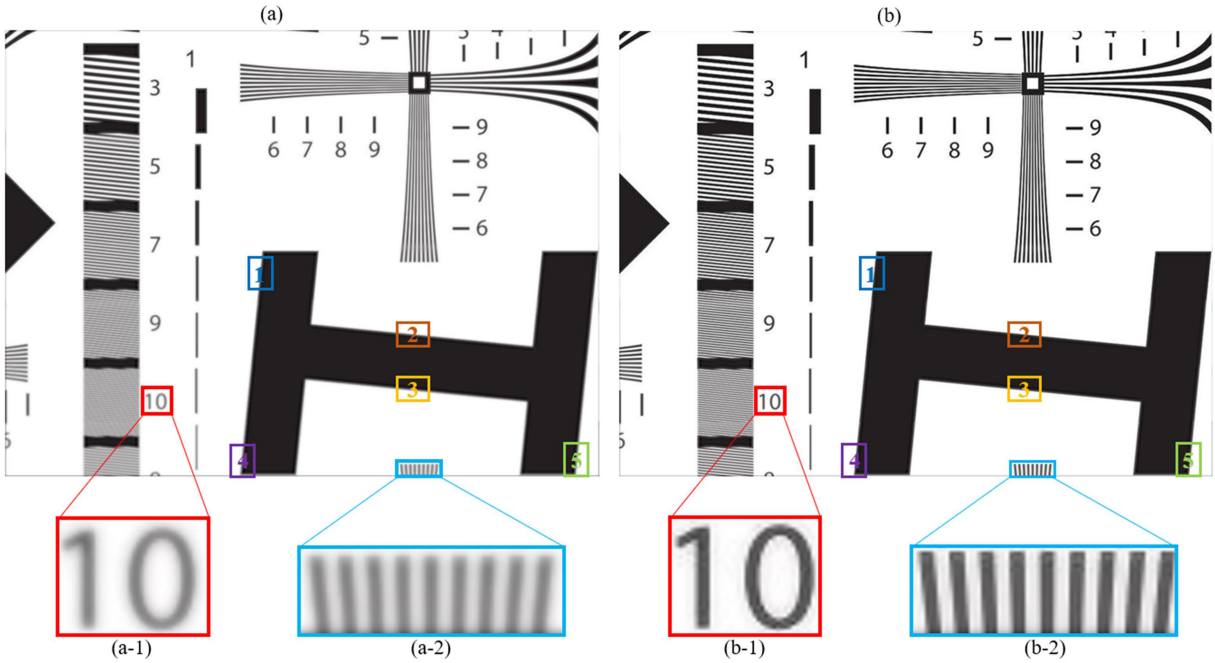

Fig. 11. Contrast before and after image restoration of resolution version. (a) Resolution plate simulation imaging, (a-1) and (a-2) are the local enlarged images of (a); (b) restoration image, (b-1) and (b-2) are the local enlarged images of (b); (a) and (b) in the selected color frame areas (1–5) are the areas of MTF measured by the Slanted-Edge method.

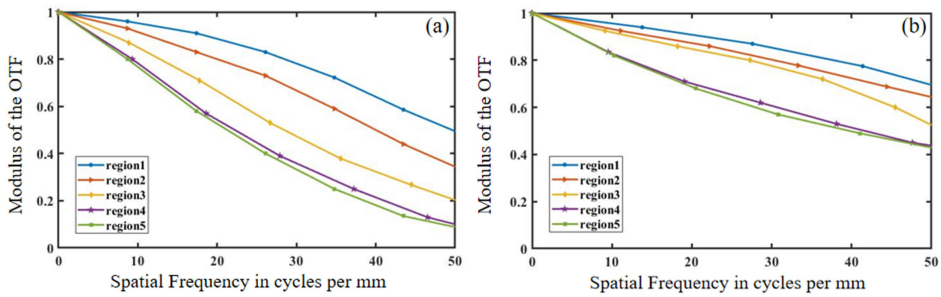

Fig. 12. Comparison of MTF before and after processing. (a) MTF of each area before processing; (b) MTF of each area after processing.

restored images, the subjective and objective aspects are evaluated, respectively. (1) Subjective evaluation: directly observing the images before and after restoration, focusing on the changes of Y field of view at −3° for preliminary comparison, as shown in Fig. 10. (2) Objective evaluation: the MTF (modulation transfer function: The ratio of the contrast of the output image to the contrast of the input image) was measured and compared before and after restoration by the Slanted-Edge method [34]–[36], as shown in Fig. 11.

Fig. 10 (a-1) is captured by the author, and (b-1) is obtained by optical system simulations. Fig. 10 (b-1) shows that the image is gradually blurred from top to bottom, especially the lowest detailed recognition is very low (corresponding Y field of view is −3°). The imaging quality of the off-axis three-mirror optical system is low in the large field of view. Compared to fig. 10 (b-1), the processed image in fig. 10 (c-1) is clearer and sharper, and the detailed recognition is improved, as shown in figs. 10 (c-2) (c-3) (c-4). This method can realize the large field of view (Y) imaging of the off-axis three-mirror optical system.

Fig. 11 is a simulation test of the partial area of the ISO12233 resolution board. Figs. 11(a) and 12(b) are the restoration image of the image. Fig. 11(a-1) and (a-2) are the partially enlarged drawings of Fig. 11(a) and Fig. 11(b-1) and (b-2) are the partially enlarged drawings of Fig. 11(b). Comparing these two images shows that the processed image is sharper with clear lines and easy to distinguish.

In order to objectively evaluate the imaging quality, five regions in Fig. 11(a) and (b) are selected, and the MTF is measured using the Slanted-Edge method. The MTF of each region is shown in Fig. 12.

Fig. 12 shows that the MTF of each region is significantly improved after restoration. This indicates that the computational imaging method proposed in this paper can effectively improve the imaging quality of the off-axis three-mirror optical system with a large field of view (Y field of view) and realizes the rectangular field of view imaging of the off-axis three-mirror optical system.

V. Conclusion

A computational imaging design method is proposed based on joint image restoration to expand the Y-direction field of

view of the off-axis three-mirror optical system and realize the rectangular field of view imaging of the off-axis three-mirror optical system. An off-axis three-mirror optical system with a focal length of 260 mm, f-number of 2.5, and field of view of 8° × 1° is simulated using the proposed method. By analyzing the aberration characteristics of the system, the PSF model is constructed based on the wavefront aberration theory and Zernike polynomials, and the image is processed by a spatial variation deconvolution algorithm. The processed image is compared with the unprocessed image, and the processed image has a clear contour. The overall imaging quality is improved, and the field of view is increased to 8° × 6° without using a freeform surface. The purpose of expanding the field of view in the Y-direction of the off-axis optical system is realized, which provides a new idea for designing an off-axis reflective optical system. In the future, this method may be applied to more systems, such as helmet mounted display, adaptive optics system and so on. About algorithm, we can apply more advanced algorithms such as neural network algorithm to improve the processing accuracy and speed

REFERENCES

[1] Z. An, X. Meng, X. Ji, X. Xu, and Y. Liu, "Design and performance of an off-axis free-form mirror for a rear mounted augmented-reality head-up display system," *IEEE Photon. J.*, vol. 13, no. 1, Feb. 2021, Art. no. 7000215.

[2] K. Fuerschbach, G. E. Davis, K. P. Thompson, and J. P. Rolland, "Assembly of a freeform off-axis optical system employing three φ-polynomial Zernike mirrors," *Opt. Lett.*, vol. 39, no. 10, pp. 2896–2899, May 2014.

[3] E. M. Schiesser, A. Bauer, and J. P. Rolland, "Effect of freeform surfaces on the volume and performance of unobscured three mirror imagers in comparison with off-axis rotationally symmetric polynomials," *Opt. Exp.*, vol. 27, no. 15, pp. 21750–21765, Jul. 2019.

[4] T. Yang, D. Cheng, and Y. Wang, "Direct generation of starting points for freeform off-axis three-mirror imaging system design using neural network based deep-learning," *Opt. Exp.*, vol. 27, no. 12, pp. 17228–17238, Jun. 2019.

[5] D. Korsch, "Design and optimization technique for three-mirror telescopes," *Appl. Opt.*, vol. 19, no. 21, pp. 3640–3645, Nov. 1980.

[6] L. G. Cook, "Three mirror anastigmatic optical system," U. S. Patent 4 265 510, May 16, 1981.

[7] R. B. Johnson, "Wide field of view three-mirror telescopes having a common optical axis," *Opt. Eng.*, vol. 27, no. 12, 1988, Art. no. 121046.

[8] G. Moretto and J. R. Kuhn, "Off-axis systems for 4-m class telescopes," *Appl. Opt.*, vol. 37, no. 16, pp. 3539–3546, Jun. 1998.

[9] A. Hammar, W. Park, S. Chang, S. Pak, A. Emrich, and J. Stake, "Wide-field off-axis telescope for the mesospheric airglow/aerosol tomography spectroscopy satellite," *Appl. Opt.*, vol. 58, no. 6, pp. 1393–1399, Feb. 2019.

[10] Q. Meng, H. Wang, K. Wang, Y. Wang, Z. Ji, and D. Wang, "Off-axis three-mirror freeform telescope with a large linear field of view based on an integration mirror," *Appl. Opt.*, vol. 55, no. 32, pp. 8962–8970, Nov. 2016.

[11] Y. Ning *et al.*, "Freeform surface graded optimization of deformable mirrors in integrated zoom and image stabilization system through vectorial ray tracing and image point freezing method," *IEEE Photon. J.*, vol. 12, no. 1, Feb. 2020.

[12] R. A. Hicks, "Controlling a ray bundle with a free-form reflector," *Opt. Lett.*, vol. 33, no. 15, pp. 1672–1674, Aug. 2008.

[13] T. Y. Zhu and G. Jin, "Design method of surface contour for a freeform lens with wide linear field-of view," *Opt. Exp.*, vol. 21, no. 22, pp. 26080–26092, Nov. 2013.

[14] K. Fuerschbach, J. P. Rolland, and K. P. Thompson, "A new family of optical systems employing φ-polynomial surfaces," *Opt. Exp.*, vol. 19, no. 22, pp. 21919–21928, Oct. 2011.

[15] J. Zhu, W. Hou, X. Zhang, and G. Jin, "Design of a low F-number freeform off-axis three-mirror system with rectangular field-of-view," *J. Opt.*, vol. 17, no. 1, Dec. 2014, Art. no. 015605.

[16] J. Liu, P. Benítez, and J. C. Miñano, "Single freeform surface imaging design with unconstrained object to image mapping," *Opt. Exp.*, vol. 22, no. 25, pp. 30538–30546, Dec. 2014.

[17] E. Hugot *et al.*, "A freeform-based, fast, wide-field, and distortion-free camera for ultralow surface brightness surveys," in *Proc. SPIE*, 2014, vol. 9143, Art. no. 91434X.

[18] E. Muslimov *et al.*, "Combining freeform optics and curved detectors for wide field imaging: A polynomial approach over squared aperture," *Opt. Exp.*, vol. 25, no. 13, pp. 14598–14610, Jun. 2017.

[19] J. P. Rolland *et al.*, "Freeform optics for imaging," *Optica*, vol. 8, no. 2, pp. 161–176, Feb. 2021.

[20] D. Kundur and D. Hatzinakos, "Blind image deconvolution," *IEEE Signal Process. Mag.*, vol. 13, no. 3, pp. 43–64, May 1996.

[21] M. R. Banham and A. K. Katsaggelos, "Digital image restoration," *IEEE Signal Process. Mag.*, vol. 14, no. 2, pp. 24–41, Mar. 1997.

[22] A. R. Harvey, O. Cossairt, J. Ke, E. Y. Lam, and P. Rangarajan, "Computational optical sensing and imaging: Feature issue introduction," *Opt. Exp.*, vol. 28, no. 12, pp. 18131–18134, Jun. 2020.

[23] X. Li, I. Lee, and S. T. Kim, "Improved integral imaging based image copyright protection algorithm using 3-D computational integral imaging pickup and super-resolution reconstruction technique," *Opt. Laser Eng.*, vol. 62, pp. 103–111, Nov. 2014.

[24] R. F. Levin, F. Durand, and W. T. Freeman, "Image and depth from a conventional camera with a coded aperture," *ACM Trans. Graph.,* vol. 26, no. 3, 2007, Art. no. 70.

[25] Y. Peng, Q. Fu, H. Amata, S. Su, F. Heide, and W. Heidrich, "Computational imaging using lightweight diffractive-refractive optics," *Opt. Exp.*, vol. 23, no. 23, pp. 31393–31407, Nov. 2015.

[26] Y. Hu, Q. Cui, L. Zhao, and M. Piao, "PSF model for diffractive optical elements with improved imaging performance in dual-waveband infrared systems," *Opt. Exp.*, vol. 26, no. 21, pp. 26845–26857, Oct. 2018.

[27] R. C. Gonzalez and R. E. Woods, *Digital Image Processing*, 3rd ed. Upper Saddle River, NJ, USA: Prentice-Hall, 2008.

[28] H. Lei, H. Feng, X. Tao, and Z. Xu, "Imaging characteristics of a wavefront coding system with off-axis aberrations," *Appl. Opt.*, vol. 45, no. 28, pp. 7255–7263, Oct. 2006.

[29] J. Lehr, J.-B. Sibarita, and J.-M. Chassery, "Image restoration in X-ray microscopy: PSF determination and biological applications," *IEEE Trans. Image Process.*, vol. 7, no. 2, pp. 258–263, Feb. 1998.

[30] F. Sroubek, J. Kamenicky, and Y. M. Lu, "Decomposition of space-variant blur in image deconvolution," *IEEE Signal Process. Lett.*, vol. 23, no. 3, pp. 346–350, Mar. 2016.

[31] D. Malacara, *Optical Shop Testing*, 3rd ed. Boca Raton, FL, USA: CRC Press, 2007.

[32] X. Hou, F. Wu, L. Yang, and Q. Chen, "Comparison of annular wavefront interpretation with Zernike circle polynomials and annular polynomials," *Appl. Opt.*, vol. 45, no. 35. pp. 8893–8901, Dec. 2006.

[33] W. Alkhaldi, D. R. Iskander, and A. M. Zoubir, "Model-order selection in Zernike polynomial expansion of corneal surfaces using the efficient detection criterion," *IEEE Trans. Biomed. Eng.*, vol. 57, no. 10, pp. 2429–2437, Oct. 2010.

[34] I. Kopriva, "Single-frame multichannel blind deconvolution by nonnegative matrix factorization with sparseness constraints," *Opt. Lett.*, vol. 30, no. 23, pp. 3135–3137, Dec. 2005.

[35] K. Masaoka, T. Yamashita, Y. Nishida, and M. Sugawara, "Modified slanted-edge method and multidirectional modulation transfer function estimation," *Opt. Exp.*, vol. 22, no. 5, pp. 6040–6046, Mar. 2014.

[36] X. Xie, H. Fan, A. Wang, N. Zou, and Y. Zhang, "Regularized slanted-edge method for measuring the modulation transfer function of imaging systems," *Appl. Opt.*, vol. 57, no. 22, pp. 6552–6558, Aug. 2018.

[37] T. Li, H. Feng, and Z. Xu, "A new analytical edge spread function fitting model for modulation transfer function measurement," *Chin. Opt. Lett.*, vol. 9, no. 3, Mar. 2011, Art. no. 031101.

[38] Y. L. Zhang, X. Wang, Z. P. Su, H. X. Pan, X. T. Chen, and W. Y. Zhang, "Freeform optical surface design in an off-axis reflective imaging system by a double seed curve extension algorithm," *Appl. Opt.*, vol. 60, no. 4, pp. 942–948, Feb. 2021.

[39] L. Chen *et al.*, "Construction of freeform mirrors for an off-axis telecentric scanning system through multiple surfaces expansion and mixing," *Results Phys.*, vol. 19, Dec. 2020, Art. no. 103354.

[40] J. Ye, L. Chen, X. Li, Q. Yuan, and Z. Gao, "Review of optical freeform surface representation technique and its application," *Opt. Eng.*, vol. 56, no. 11, Nov. 2017, Art. no. 110901.

[41] W. J. Smith, *Modern Optical Engineering*, 4th ed. New York, NY, USA: McGraw Hill, 2008.